Latin American Journal of Solids and Structures
www.lajss.org

Dynamic Response of Orthotropic Membrane Structure under Impact Load based on Multiple Scale Perturbation Method

Abstract

This paper investigates the dynamic response of rectangular prestressed membrane subjected to concentrated impact load based on multiple scale perturbation method. The governing equations of motion of nonlinear vibration are derived based on the Föppl large deflection theory and Galerkin method. By introducing different time scales to consider the process of vibration, the results of dynamic response are obtained by applying the multiple scale perturbation method. Furthermore, the effects of pretension force, velocity of load and dimension of membrane on the dynamic response of membrane are discussed. The present work studies the problem of the dynamic response of prestressed membrane subjected to concentrated impact load in different time scales, and provides a more accurate theoretical model for design of membrane structure.

Keywords

Membrane structure; dynamic response; nonlinear vibration; multiple scale perturbation method.

Z. L. Zheng [a, b, c]
C. Y. Liu [d]
D. Li [a]
T. Zhang [a]

[a] School of Civil Engineering, Chongqing University, 400045, Chongqing, China, zhengzl@cqu.edu.cn
[b] Key Laboratory in Mountain Area, Chongqing University, 400045, Chongqing, China
[c] Chongqing Jian Zhu College, 400072, Chongqing, China
[d] Urban Railway and Architecture Design Institute, China Railway First Survey & Design Institute, 710043, Xi'an, China

http://dx.doi.org/10.1590/1679-78253835

Received 15.03.2017
In revised form 05.06.2017
Accepted 05.06.2017
Available online 17.06.2017

1 INTRODUCTION

Membrane structures have been widely applied to construction engineering, aerospace engineering, mechanical engineering and other fields. In all of these engineering fields, it is inevitable to solve the vibration problems of membrane structures, especially for the case subjected to impact load such as hailstone, falling object and rainstorm, in which case the membrane structure may fail to perform the basic function, even structural destruction (Young et. al, 2005; Balkan and Mecitoglu, 2014). Thus, it is necessary to study the dynamic response of membrane structure under impact load.

In recent decades, the dynamic response of membrane structure under impact load has been widely investigated. Hallquist and Feng (1975) investigated the dynamic response of a uniform circular membrane subjected to a step pressure loading. The nonlinear second-order ordinary differential equations were established by applying the principle of virtual work, and sought by the Rayleigh-Ritz method. The results are solved by an implicit Newmark time integration scheme with the Newton-Raphson iterative technique. K. Nagaya (1978) treated the problem of finding the response to dynamic loads of a membrane with arbitrary shape. The boundary condition was expanded into a Fourier series, and the general solution of motion equation was obtained by the Laplace transform. Haddow et al. (1992) considered the finite amplitude wave propagation in a circular isotropic membrane under a suddenly applied pressure. The governing equations in Lagrangian form were sought by the method of characteristics and a finite difference scheme. Kapoor et al. (2006) developed a finite element model of the flexible membrane structures to blast loads. Transient analysis was performed based on the Newmark method and Newton-Raphson method. Consequently, the displacement time histories and dynamic stresses were computed. Zheng et al. (2012) established the governing equations of vibration for orthotropic membrane under impact load based on the Föppl large deflection. The complex factors such as the geometrical nonlinearities, air damping and orthotropic property of material were considered. The equations were solved by applying the power series method and L-P/KBM perturbation method, and the results such as frequency and displacement time histories were obtained. Yang and Sultan (2016) introduced tensegrity-membrane systems, which were composed of bars, tendons and membranes, and studied the system dynamics based on the nonlinear finite element method. Simulations based on the dynamic relaxation technique were presented to understand the membrane behavior.

In a word, a variety of methods, such as point collocation method (Kolsti and Kunz, 2013), finite element method (Chakravarty, 2012; Aksoylar et. al, 2012), variation principle (Eshmatov, 2007), Rayleigh-Ritz (Belytschko and Lu, 1994), and perturbation method have been applied to investigate the problem of dynamic response of membrane structure under impact load (Liu et. al, 2010). These methods are all derived and applied based on a single time scale, which can be used to describe the progress of vibration in the faster time scale such as 1s, 2s, ... However, the interaction time between the impact load and membrane is remarkably short, and it has a difficulty in evaluating the vibration during interaction using only one time scale. Thus, another time scale is needed to introduce to describe the progress of vibration during impact progress in the lower time scale such as 0.001s, 0.002s... Then, the analytical result obtained can achieve higher accuracy, and the improved algorithm can be applied in the field of design and maintenance (Greschik and Mikulas, 2012).

In this paper, the objectives are to study the dynamic response of the orthotropic membrane subjected to impact load using two time scales, and to propose a more accurate prediction method for estimating the dynamic behavior of membrane under impact load. The governing equations of motion are established based on the Föppl large deflection theory, and uncoupled by the Galerkin method. Then, the multiple scale perturbation method is applied to solve the uncoupled equations. Consequently, the analytical results of dynamic response are obtained. By comparing the theoretical results and experimental value, the theoretical model is validated. Furthermore, the effects of pa-

rameters such as pretension force, velocity of load and dimensions of membrane on the dynamic response are discussed.

2 THEORETICAL STUDY

2.1 Formulation of the Problem

The loading configuration is illustrated in Fig. 1. The x-axis and y-axis are along the in-plane directions and z-axis is along the thickness direction. An orthotropic rectangular membrane of thickness h and area with the length of a and the width of b is prestressed bi-axially normal to each edge. The pretension force along the directions of x and y is N_{0x} and N_{0y}, respectively. Then, the stretched membrane is subjected to uniform impact load. The impact load is represented by a pellet, which has the velocity of v_0 and the mass of M.

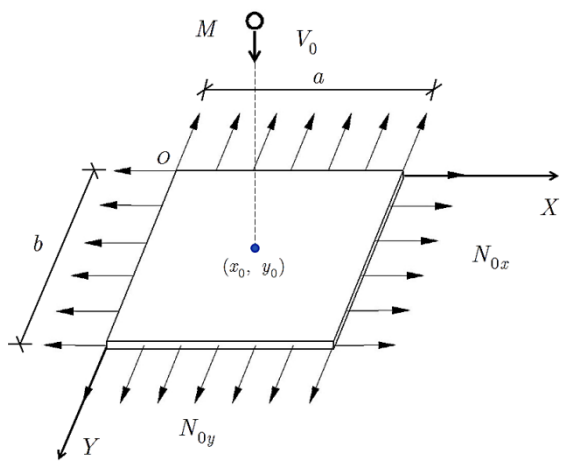

Figure 1: The rectangular membrane impact model.

The position of impact load is located at the point $(x_0,\ y_0)$, and it can be expressed as :

$$p(x,y,t) = F(t)\delta(x-x_0)(y-y_0) \tag{1}$$

where: $F(t)$ denotes the impact load; $\delta(x)$ is the Dirac function.

The simply supported boundary can be described as:

$$\begin{cases} w\left(0,y,t\right)=0 \\ w\left(a,y,t\right)=0 \end{cases}, \quad \begin{cases} w\left(x,0,t\right)=0 \\ w\left(x,b,t\right)=0 \end{cases} \tag{2a,b}$$

where: w is the deformation of out-plane on membrane; t is the time of dynamic response.

The membrane remains a plane before the impact load contacts. After the impact load contacts the membrane, the system formed by the load and membrane starts to move together. Therefore, the following initial conditions for the membrane:

$$w(x_0,y_0,t)\big|_{t=0}=0,\quad \frac{\partial w(x_0,y_0,t)}{\partial t}\big|_{t=0}=v_0' \tag{3}$$

According to the momentum theorem, the relation between impact load and deformation of membrane can be expressed as:

$$F(t)=-M\frac{\partial w^2(x_0,y_0,t)}{\partial t^2} \tag{4}$$

2.2 Dynamic Governing Equations

According to the Föppl large deflection theory and D's Alembert's principle, the damped forced vibration motion equation and consistency equation of orthotropic membrane can be derived as:

$$\begin{cases}\rho\dfrac{\partial^2 w}{\partial t^2}+c\dfrac{\partial w}{\partial t}-(N_x+N_{0x})\dfrac{\partial^2 w}{\partial x^2}-(N_y+N_{0y})\dfrac{\partial^2 w}{\partial y^2}=p(x,y,t)\\ \dfrac{1}{E_1}\dfrac{\partial^4\varphi}{\partial y^4}+\dfrac{1}{E_2}\dfrac{\partial\varphi^4}{\partial x^4}=(\dfrac{\partial^2 w}{\partial x\partial y})^2-\dfrac{\partial^2 w}{\partial x^2}\dfrac{\partial^2 w}{\partial y^2}\end{cases} \tag{5a,b}$$

where: E_1 and E_2 are Young's modulus in x and y direction, respectively; N_{0x} and N_{0y} are initial tension in x and y direction, respectively; N_x and N_y are additional tension in x and y direction, respectively; ρ is the aerial density of membrane; c is coefficient of damping; φ is the stress function.

The stress functions are introduced as followings:

$$\begin{cases}N_x=\sigma_x h=h\dfrac{\partial^2\varphi}{\partial y^2},\quad N_{0x}=h\sigma_{0x}\\ N_y=\sigma_y h=h\dfrac{\partial^2\varphi}{\partial x^2},\quad N_{0y}=h\sigma_{0y}\end{cases} \tag{6}$$

The functions that satisfy the boundary conditions Eq. (2) are as (Eshmatov, 2007):

$$w(x,y,t)=\sum_{m=1}^{\infty}\sum_{n=1}^{\infty}T_{mn}(t)W_{mn}(x,y) \tag{7}$$

and

$$\varphi(x,y,t)=\sum_{m=1}^{\infty}\sum_{n=1}^{\infty}\phi_{mn}(x,y)T^2{}_{mn}(t) \tag{8}$$

where: $W_{mn}(x,y)$ is the mode shape function; $\phi_{mn}(x,y)$ and $T_{mn}(t)$ are undetermined functions.

The mode shape function can be assumed as:

$$W_{mn}(x,y)=\sin\frac{m\pi x}{a}\sin\frac{n\pi y}{b} \tag{9}$$

where: m and n are integer, and denote the sine half-wave number in x and y, respectively.

By substituting Eqs. (7-9) into Eq. (5b), one obtains:

$$\frac{1}{E_1}\frac{\partial^4\phi}{\partial y^4}+\frac{1}{E_2}\frac{\partial^4\phi}{\partial x^4}=\frac{m^2n^2\pi^4}{2a^2b^2}(\cos\frac{2m\pi x}{a}+\cos\frac{2n\pi y}{b}) \tag{10}$$

Assume the solution of Eq. (10) as followings:

$$\phi(x,y)=\alpha\cos\frac{2m\pi x}{a}+\beta\cos\frac{2n\pi y}{b}+\gamma_1x^3+\gamma_2x^2+\gamma_3y^3+\gamma_4y^2 \tag{11}$$

By substituting Eq. (11) into Eqs. (2) and (10), one can obtain:

$$\alpha=\frac{E_2n^2a^2}{32m^2b^2},\ \beta=\frac{E_1m^2b^2}{32n^2a^2},\ \gamma_1=\gamma_3=0,\ \gamma_2=\frac{\pi^2E_2n^2}{16b^2},\ \gamma_4=\frac{\pi^2E_1m^2}{16a^2}$$

By substituting Eqs. (7-8) into Eq. (5a), the expression according to the Galerkin method (Liu et. al, 2013) can be obtained as:

$$\begin{aligned}&\int_0^a\int_0^b[\rho W^2\frac{d^2T(t)}{dt^2}+cW^2\frac{dT(t)}{dt}-(N_{0x}\frac{\partial^2W}{\partial x^2}W+N_{0y}\frac{\partial^2W}{\partial y^2}W)T(t)\\&-h(\frac{\partial^2\phi}{\partial y^2}\frac{\partial^2W}{\partial x^2}W+\frac{\partial^2\phi}{\partial x^2}\frac{\partial^2W}{\partial y^2}W)T^3(t)]dxdy=\int_0^a\int_0^b[F(t)\delta(x-x_0)(y-y_0)W]dxdy\end{aligned} \tag{12}$$

The Eq. (12) can be handled as:

$$\begin{aligned}&\frac{d^2T(t)}{dt^2}+\frac{c}{\rho}\frac{dT(t)}{dt}+\frac{m^2\pi^2b^2N_{0x}+n^2\pi^2a^2N_{0y}}{\rho a^2b^2}T(t)\\&+\frac{2m^2n^2\pi^4h\beta+2m^2n^2\pi^4h\alpha}{\rho a^2b^2}T^3(t)=\frac{4}{\rho ab}F(t)\sin\frac{m\pi x_0}{a}\sin\frac{n\pi y_0}{b}\end{aligned} \tag{13}$$

By substituting Eq. (4) into Eq. (13), one can introduce the little parameter $\varepsilon=h\varepsilon=h^2/ab\ll1$ and replace $T(t)$ with $y(t)$. The simplified expression is obtained as following:

$$\ddot{y}+w_0^2y=\varepsilon(\alpha_1y^3+\alpha_2\dot{y}) \tag{14}$$

where: $\ddot{y}=\frac{d^2y}{dt^2}$; $\dot{y}=\frac{dy}{dt}$; $\alpha_1=\frac{-2m^2n^2\pi^4(\alpha+\beta)}{h(\rho ab+4M\sin^2\frac{m\pi x_0}{a}\sin^2\frac{n\pi y_0}{b})}$;

$\alpha_2=\frac{-ca^2b^2}{h^2(\rho ab+4M\sin^2\frac{m\pi x_0}{a}\sin^2\frac{n\pi y_0}{b})}$.

2.3 Solutions of Governing Equations

Different from the only one time scale such as 1s, 2s, ..., applied to solve the vibration problem (Nayfeh, 1981), this paper introduces another slower time scale such as 0.001s, 0.002s, ..., and utilizes two time scales to solve the vibration problem based on the multiple scale perturbation method (Belytschko and Lu, 1994). The complex vibration problem can be handled more accurately by means of selecting two time scales. Besides the original scale $T_0 = t$, the other slower scale $T_1 = \varepsilon t$ is introduced. Thus, the corresponding derivative can be obtained as:

$$\begin{cases} \dfrac{d}{dt} = D_0 + \varepsilon D_1 + ..., & \text{(a)} \\ \dfrac{d^2}{dt^2} = D^2{}_0 + 2\varepsilon D_0 D_1 + ... & \text{(b)} \end{cases} \tag{15a,b}$$

Expand $T(t)$ in terms of ε as:

$$T(t) = u(T) = u_0(T_0, T_1) + \varepsilon u_1(T_0, T_1) \tag{16}$$

By submitting Eq. (16) into Eq. (14), one can obtain:

$$\begin{aligned} &\frac{\partial^2 u_0}{\partial T^2{}_0} + \varepsilon \frac{\partial^2 u_1}{\partial T^2{}_0} + 2\varepsilon\left(\frac{\partial^2 u_0}{\partial T_0 \partial T_1} + \varepsilon \frac{\partial^2 u_1}{\partial T_0 \partial T_1}\right) + w^2{}_0(u_0 + \varepsilon u_1) \\ &-\varepsilon\alpha_2\left(\frac{\partial u_0}{\partial T_0} + \varepsilon \frac{\partial u_1}{\partial T_0}\right) - \varepsilon\alpha_1(u_0 + \varepsilon u_1)^3 = 0 \end{aligned} \tag{17}$$

Collect the same power of Eq. (17), and the simultaneous equations can be obtained as follows:

$$\begin{cases} \dfrac{\partial^2 u_0}{\partial T^2{}_0} + w^2{}_0 u_0 = 0 & \text{(a)} \\ \dfrac{\partial^2 u_1}{\partial T^2{}_0} + 2\dfrac{\partial^2 u_0}{\partial T_0 \partial T_1} + w^2{}_0 u_1 - \alpha_2 \dfrac{\partial u_0}{\partial T_0} - \alpha_1 u^3{}_0 = 0 & \text{(b)} \end{cases} \tag{18}$$

The general solution of Eq. (18a) can be solved as followings:

$$u_0 = A(T_1)e^{iT_0 w_0} + \overline{A}(T_1)e^{-iT_0 w_0} \tag{19}$$

where: $A = \dfrac{1}{2} D e^{i\beta}$.

By submitting Eq. (19) into Eq. (18b), one can obtain:

$$\begin{aligned} D^2{}_0 u_1 + w^2{}_0 u_1 &= (-2)(A' e^{iT_0 w_0} i w_0 - i w_0 \overline{A}' e^{-iT_0 w_0}) + \alpha_2(A e^{iT_0 w_0} i w_0 - i w_0 \overline{A} e^{-iT_0 w_0}) \\ &\quad + \alpha_1(A e^{iT_0 w_0} + \overline{A} e^{-iT_0 w_0})^3 \\ &= e^{iT_0 w_0}(-2A' i w_0 + \alpha_2 A i w_0 + 3\alpha_1 A^2 \overline{A}) + \alpha_1 A^3 e^{3iT_0 w_0} + cc \end{aligned} \tag{20}$$

where: cc stands for the conjugate complex.

The Eq. (18b) belongs to a linear equation of forced vibration. Thus, the general solution of corresponding homogeneous equation is assumed as:

$$\overline{u}_1 = Ae^{iT_0w_0} + \overline{A}e^{-iT_0w_0} \tag{21}$$

In order to eliminate the singularity of equation, the general solution term and force term have to be orthogonal, namely,

$$< \overline{u}_1, f >= \frac{1}{2\pi}\int_0^{2\pi} \overline{u}_1 f dT_0 = 0 \tag{22}$$

Furthermore, one can obtain as follows:

$$-D'iw_0 + Dw_0\beta' + \frac{1}{2}Diw_0\alpha_2 + \frac{3}{8}D^3\alpha_1 = 0 \tag{23}$$

Make the real and imaginary part be zero, respectively, and one can obtain:

$$\begin{cases} \beta' Dw_0 + \dfrac{3}{8}D^3\alpha_1 = 0 \\ -D'w_0 + \dfrac{1}{2}Dw_0\alpha_2 = 0 \end{cases} \tag{24}$$

The solutions of Eq. (24) are as follows:

$$\begin{cases} \beta = -\dfrac{3}{8}\dfrac{D^2}{w_0}\alpha_1 T_1 + C_1 \\ D = e^{0.5\alpha_2 T_1}C_2 \end{cases} \tag{25}$$

Then, the solution of u_1 is as follows:

$$u_1 = D\cos(T_0w_0 + \beta) - \frac{1}{32}\frac{1}{w^2{}_0}\alpha_1 D^3\cos(3\beta + 3T_0w_0) \tag{26}$$

By submitting Eqs. (19) and (26) into Eq. (16), the displacement function is obtained as:

$$u = u_0 + \varepsilon u_1 = D\cos(T_0w_0 + \beta)(1+\varepsilon) - \frac{\varepsilon}{32}\frac{1}{w^2{}_0}\alpha_1 D^3\cos(3\beta + 3T_0w_0) \tag{27}$$

Consider the initial condition as follows:

$$u(t)\big|_{t=0} = b_0,\ \frac{du(t)}{dt}\Big|_{t=0} = v_0' \tag{28}$$

where: b_0 and v_0' are initial displacement and velocity, respectively.

Based on the initial condition Eq. (28), one can obtain:

$$\begin{cases} \beta = -\dfrac{3}{8}\dfrac{e^{\alpha_2 \varepsilon t} {v_0}^2}{{w_0}^3}\alpha_1 t\varepsilon + \dfrac{\pi}{2} \\ D = e^{0.5\alpha_2 \varepsilon t}\dfrac{{v_0}'}{w_0} \end{cases} \tag{29}$$

By submitting Eq. (29) into Eq. (27), the displacement function varying with time is obtained as follows:

$$\begin{aligned} u = u_0 + \varepsilon u_1 = {} & e^{0.5\alpha_2 \varepsilon t}\frac{v_0'}{w_0}\cos(tw_0 - \frac{3}{8}\frac{1}{w_0}e^{\alpha_2 \varepsilon t}(\frac{v_0'}{w_0})^2\alpha_1 \varepsilon t + \frac{\pi}{2})(1+\varepsilon) \\ & -\frac{\varepsilon}{32}\frac{1}{{w^2}_0}\alpha_1 e^{1.5\alpha_2 \varepsilon t}(\frac{v_0'}{w_0})^3\cos(3tw_0 - \frac{9}{8}\frac{1}{w_0}e^{\alpha_2 \varepsilon t}(\frac{v_0'}{w_0})^2\alpha_1 \varepsilon t + \frac{3\pi}{2}) \end{aligned} \tag{30}$$

By submitting Eq. (30) into Eq. (7), the displacement function varying with time and space is obtained:

$$\begin{aligned} w(x,y,t) = {} & \sum_{m=1}^{\infty}\sum_{n=1}^{\infty}\sin\frac{m\pi x}{a}\sin\frac{n\pi y}{b} \\ & \bullet \begin{cases} e^{0.5\alpha_2 \varepsilon t}\dfrac{v_0'}{w_0}\cos(tw_0 - \dfrac{3}{8}\dfrac{1}{w_0}e^{\alpha_2 \varepsilon t}(\dfrac{v_0'}{w_0})^2\alpha_1 \varepsilon t + \dfrac{\pi}{2})(1+\varepsilon) \\ -\dfrac{\varepsilon}{32}\dfrac{1}{{w^2}_0}\alpha_1 e^{1.5\alpha_2 \varepsilon t}(\dfrac{v_0'}{w_0})^3\cos(3tw_0 - \dfrac{9}{8}\dfrac{1}{w_0}e^{\alpha_2 \varepsilon t}(\dfrac{v_0'}{w_0})^2\alpha_1 \varepsilon t + \dfrac{3\pi}{2}) \end{cases} \end{aligned} \tag{31}$$

The Eq. (31) presents the displacement-time relationship at any point during free vibration. By taking the first and second derivative of Eq. (31), the corresponding velocity and acceleration can be obtained.

3 VERIFICATION WITH AN EXISTING MEMBRANE EXPERIMENT

The experiment (Guo et. al, 2015) can be used to validate the analytical result. investigated the vibration of orthotropic rectangle membrane under impact load. The rectangle membrane, which has the plane dimension 1200 mm×1200 mm, was prestressed by the biaxial tensile stent. The tension in both directions was equal. The pretension force in the experimental scheme was divided into eight grades, followed by 1 kN, 2 kN, 3 kN, 4 kN, 5 kN, 6 kN, 7 kN and 8 kN. The Heytex membrane as a brand of membrane building material is selected. The density of the membrane is 0.95 kg/m^2, and the thickness of the membrane is 0.8 mm. The material property of the membrane is orthotropic, which has the elastic modulus of 1720 Mpa along the warp direction and the elastic modulus of 1490 Mpa along the zonal direction. The impact load was simulated by a pellet. The radius of the pellet was 2.5 mm, and the mass of the pellet was 0.88 g. The vibration of membrane was collected and tracked by the noncontact laser displacement.

The comparison of displacement histories curves obtained from theory with that obtained from experiment was presented in Fig. 2.The vibration condition was that the membrane was subjected to the pellet with 10 m/s velocity as the pretension force was 1 kN, 3 kN, 5 kN and 7kN. It can be seen that the process of vibration calculated from the proposed theoretical model shows good con-

sistence with that obtained from experimental measurement, which means that the theoretical model can describe the process of vibration accurately. In addition, Fig. 3 shows theoretical results and experimental data on the maximal amplitude of membrane under the pretension force of 3 kN. Compared with the theoretical results using single time scale (Liu et. al, 2013), namely KBM perturbation method, the theoretical results using two time scales in this paper, namely multiple scale perturbation method matches better with that obtained from experiment. As is expected, the results in zero order can achieve a high precision.

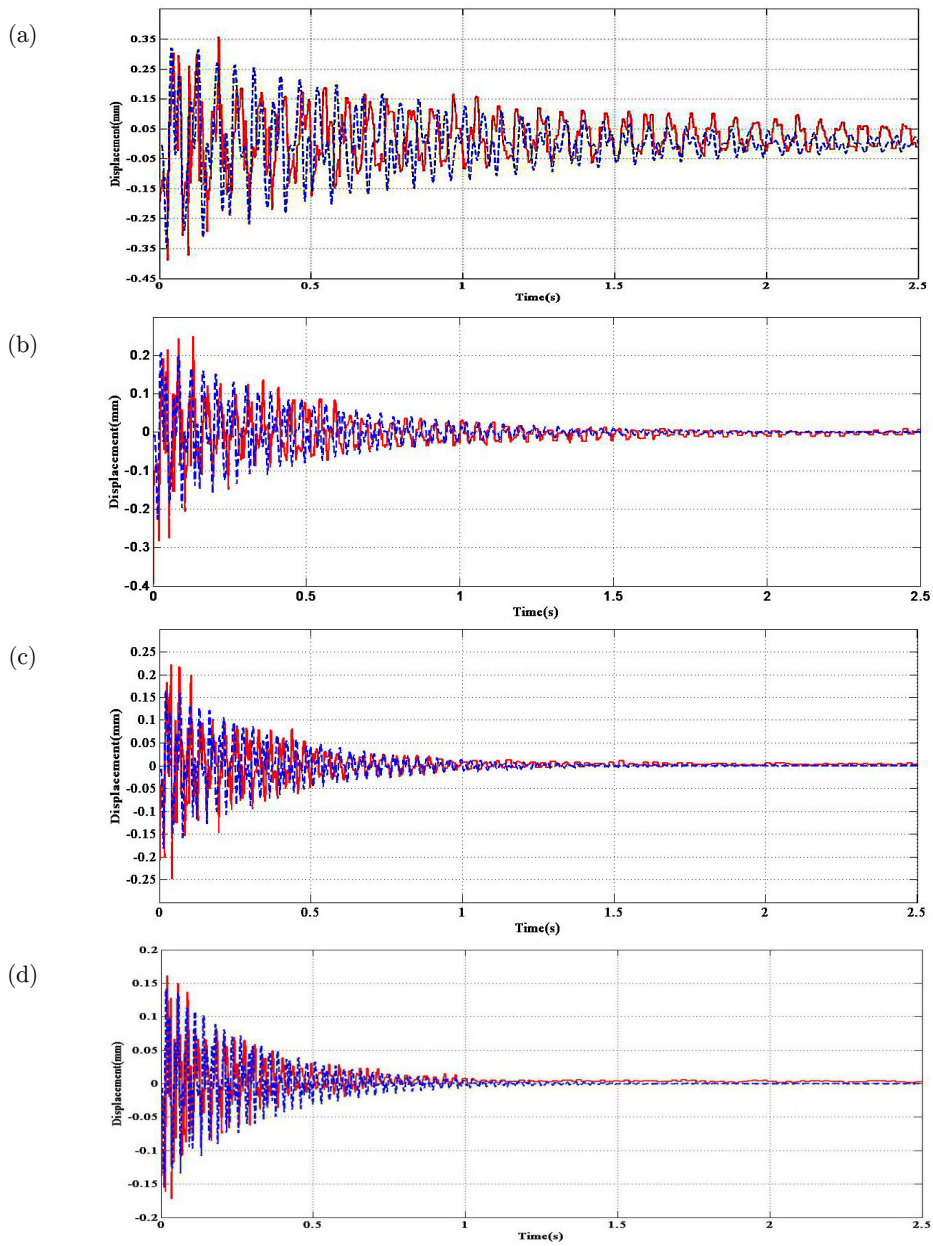

Figure 2: Comparison of the displacement histogram between theoretical and experimental results: (a) 1kN; (b) 3kN; (c) 5kN; (d) 7kN.

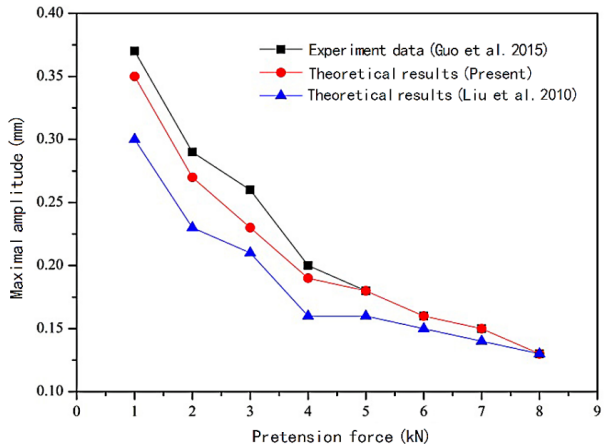

Figure 3: Comparison of the maximal amplitude between theoretical and experimental results.

4 RESULTS AND DISCUSSION

4.1 Effects of Pretension Force on Dynamic Response

4.1.1 Effect of Pretension Force on Maximal Amplitude of Vibration

Fig. 4 presents the relationship between maximal amplitude and pretension force. It can be found that the theoretical results fit well with experimental data. As is shown, the maximal amplitude increases significantly with the pretension force increasing within the range of 4 kN pretension force. When the pretension force varies over 4kN pretension force, the maximal amplitude tends to stable, and the influence of pretension force on maximal amplitude becomes little. The reason for this phenomenon is that the rigidity of outside plane is provided by the pretension force on the boundary (Jenkins and Korde, 2006). The rigidity of outside plane increases with the pretension force increasing. Thus, the dynamic response of membrane including the maximal amplitude decreases accordingly.

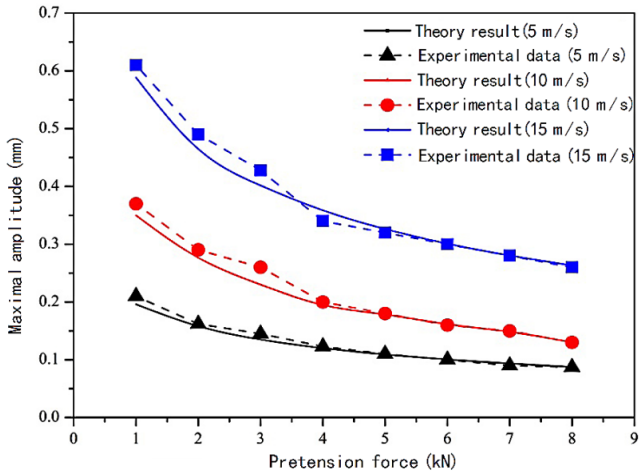

Figure 4: Maximal amplitude of vibration at center point curves versus pretension force with different velocity of impact load.

4.1.2 Effect of Pretension Force on Maximal Velocity of Vibration

Fig. 5 presents the relationship between maximal amplitude and pretension force. It can be found that the theoretical results fit well with experimental data. As is shown, the maximal amplitude increases significantly with the pretension force increasing within the range of 4 kN pretension force. When the pretension force varies over 4kN pretension force, the maximal amplitude tends to stable, and the influence of pretension force on maximal amplitude becomes little. The reason for this phenomenon is that the rigidity of outside plane is provided by the pretension force on the boundary. The rigidity of outside plane increases with the pretension force increasing. Thus, the dynamic response of membrane including the maximal amplitude decreases accordingly.

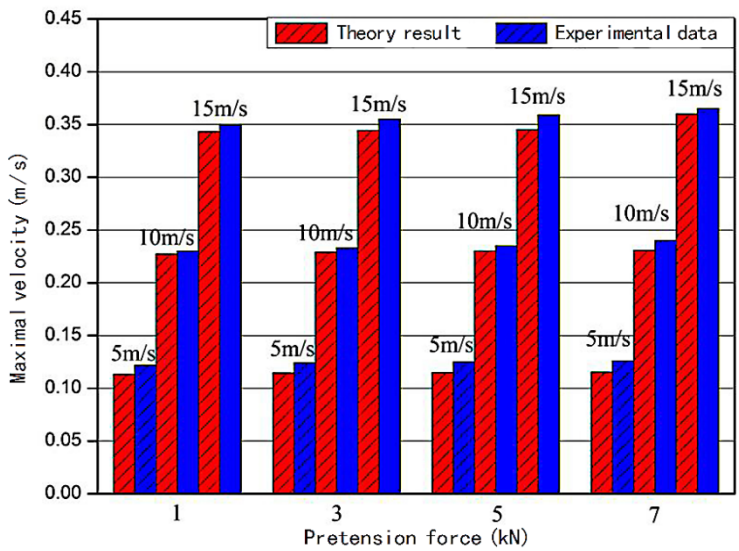

Figure 5: Maximal velocity of vibration at center point curves versus pretension force with different velocity of impact load.

4.1.3 Effect of Pretension Force on Maximal Acceleration of Vibration

Table 1 lists the maximal acceleration at center point with different pretension force. By taking the second-order derivative of the Eq. (47), the theoretical result of acceleration can be obtained. Unlike the rules of velocity, the maximal acceleration increases obviously with the pretension force increasing. This can be explained that, the increasing pretension force leads to more and more localized vibration, which brings out the increasing maximal acceleration. Nevertheless, the increasing trend becomes slow gradually until stable. When the pretension force varies within 4 kN, the growth amplitude of maximal acceleration can reach 18.82 % averagely. Then, the growth amplitude drops into 8.54 % averagely with the pretension force over 4 kN. As a result, the dynamic response of membrane is more significant when the pretension force is in higher levels.

V (m/s)		Pretension force (kN)							
		1	2	3	4	5	6	7	8
5	Theory(m/s^2)	52.37	79.68	93.78	106.05	117.63	128.35	138.43	147.88
	Exp.(m/s^2)	54.25	82.65	95.28	110.32	124.32	135.65	156.20	156.95
	Error(%)	3.59	3.73	1.60	4.03	5.69	5.69	12.84	6.13
	$\Delta a/a$(%)	-	52.15	17.70	13.08	10.92	9.11	7.85	6.83
10	Theory(m/s^2)	126.05	161.37	188.65	213.07	235.83	257.14	277.27	296.12
	Exp.(m/s^2)	130.22	165.95	195.23	220.74	228.25	260.22	298.54	300.24
	Error(%)	3.31	2.84	3.49	3.60	-3.21	1.20	7.67	1.39
	$\Delta a/a$(%)	-	28.02	16.91	12.94	10.68	9.04	7.83	6.80
15	Theory(m/s^2)	197.87	246.65	286.21	322.00	354.99	386.72	416.87	445.00
	Exp.(m/s^2)	205.84	249.32	300.24	330.55	386.54	400.21	450.28	450.32
	Error(%)	4.03	1.08	4.90	2.66	8.89	3.49	8.01	1.20
	$\Delta a/a$(%)	-	24.65	16.04	12.50	10.25	8.94	7.80	6.75

Note: Δ_a denotes the difference of theoretical acceleration value between two adjacent pretension force, namely $\Delta_a = a_{F_{i+1}} - a_{F_i}$; Δ_a / a denotes the amplitude of theoretical acceleration value between two adjacent pretension force, namely $\Delta_a / a = (a_{F_{i+1}} - a_{F_i}) / a_{F_i}$.

Table 1: Verification in acceleration with different pretension force.

4.2 Effects of Velocity of Impact Load on Dynamic Response

4.2.1 Effect of Velocity of Impact Load on Maximal Amplitude of Vibration

Fig. 4 shows the maximal amplitude at center point under impact load with different velocity. The maximal amplitude increases about 64.6 % when the velocity of impact load rises from 5 m/s to 10 m/s. Then, the growth amplitude reaches about 200.1 % when the velocity of impact load rises from 5 m/s to 15 m/s. It is obvious that the effect of velocity of impact load on maximal amplitude is considerable.

4.2.2 Effect of Velocity of Impact Load on Maximal Velocity of Vibration

Fig. 5 compares the maximal velocity during vibration when the impact load is different. It can be found that the maximal velocity of vibration increases nearly linearly with the velocity of impact load becoming larger. This demonstrates that the velocity of impact load is the key factor on the maximal velocity of vibration.

4.2.3 Effect of Velocity of Impact Load on Maximal Acceleration of Vibration

Table 1 presents the maximal acceleration under impact load with different velocity. Similar to the rules of maximal velocity, the maximal acceleration increases almost linearly when the velocity of impact load becomes larger. The growth amplitude of acceleration between two adjacent pretension forces tends to be stable when the velocity of impact load is large.

4.3 Effects of Dimension on Dynamic Response

4.3.1 Effect of Dimension on Maximal Amplitude of Vibration

Fig. 6 compares the maximal amplitude of membrane with different dimension at center point. It can be seen that the maximal amplitude for square membrane with the dimension of 1200 mm×1200 mm is smaller than that for rectangle membrane with the dimension of 1200 mm×800 mm. In this occasion, the area is reduced about 33 %, and the growth amplitude of maximal amplitude of vibration is averagely 35.7 %. This is because the membrane impacted by impact load starts to vibrate. Meanwhile, the kinetic energy of impact load is transformed into potential energy of membrane by means of the deformation on outside surface. Then, the vibration continues for some time, and ends at last due to the damping. During this time, the transformation between kinetic energy and potential energy in membrane repeats along with process of vibration. The amplitude of vibration represents the potential energy. Consequently, when the vibration area of membrane is larger in same occasion, the potential energy per area is less, and the amplitude of vibration becomes smaller.

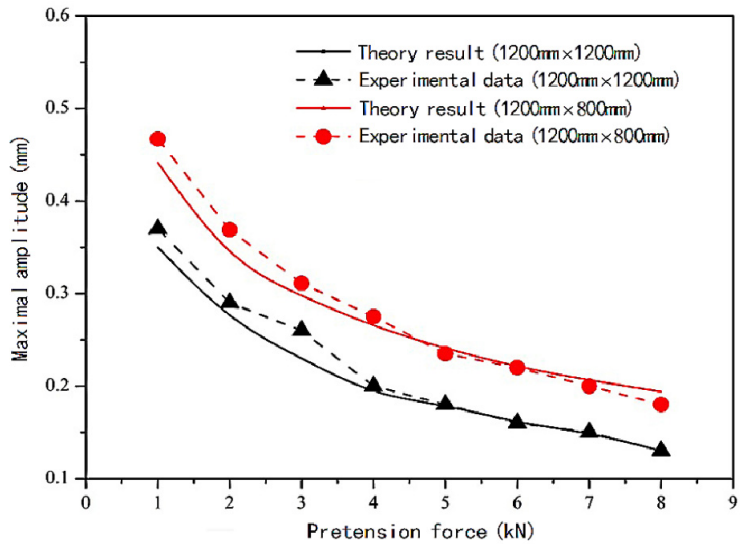

Figure 6: Maximal amplitude of vibration at center point curves versus dimension of membrane.

4.3.2 Effect of Dimension on Maximal Velocity of Vibration

Fig. 7 shows the maximal velocity of vibration at center point with different dimension. The maximal velocity of vibration increases obviously with the dimension reduces. The dimension of membrane reduces from 1200 mm×1200 mm to 1200 mm×800 mm, and the maximal velocity increases averagely 52.17 %. Similar to with the rules of amplitude, the reduction of vibration area causes the increase of potential energy per area and velocity during vibration.

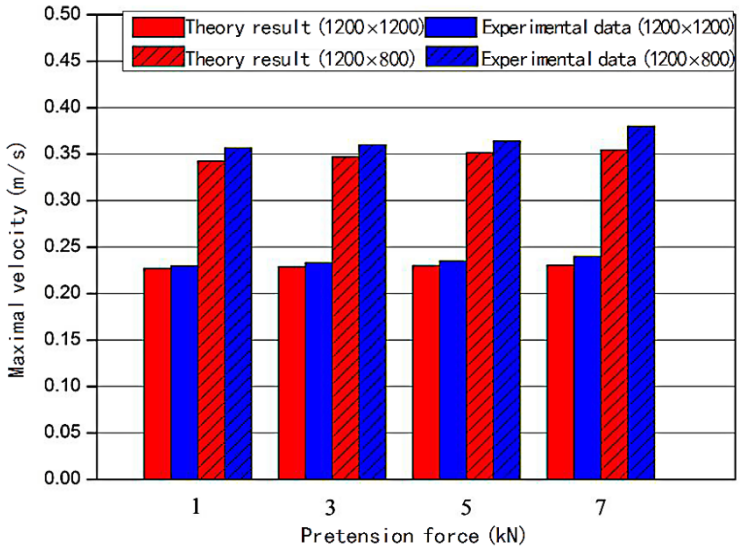

Figure 7: Maximal velocity of vibration at center point curves versus dimension of membrane.

4.3.3 Effect of Dimension on Maximal Acceleration of Vibration

Fig. 8 shows the maximal acceleration of vibration at center point with different dimension. The maximal acceleration increases averagely 106.5 % along with the reduction of area, which reduces to 1200 mm×800 mm from 1200 mm×1200 mm. The growth amplitude is significant. This can demonstrate that the dimension of membrane affects the dynamic response rather obviously.

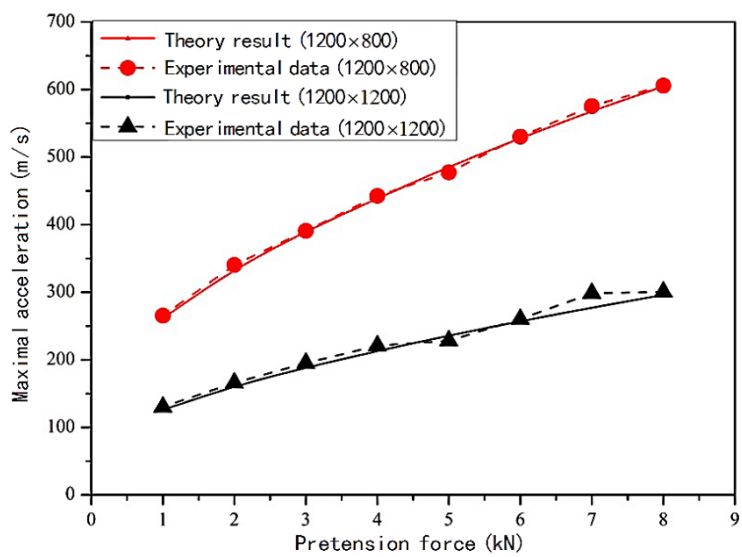

Figure 8: Maximal acceleration of vibration at center point curves versus dimension of membrane.

5 CONCLUSIONS

In this research, the dynamic response of membrane subjected to the impact load was studied. The vibration governing equations were derived by the Föppl large deflection theory, and simplified by the Galerkin method. Then, the multiple-scale perturbation method is applied to solve the simplified vibration equations by introducing different time scales. Consequently, the analytical solutions of dynamic response parameters, such as maximal displacement, amplitude, velocity, acceleration, were obtained. Some significant conclusions can be drawn as following:

- •The theoretical model proposed can predict the dynamic response of the rectangular prestressed membrane subjected to concentrated impact load accurately.
- •When the pretension force varies within 4kN, the maximal amplitude of vibration reduces obviously with the pretension force increasing. However, when the pretension force exceeds over 4kN, the maximal amplitude tends to be stable with the increase of pretension force. Moreover, the increase of pretension force can lead to the local vibration. Thus, the maximal acceleration increases obviously.
- •The dynamic response of membrane is affected significantly by velocity of impact load. Each parameter increases almost linearly along with the increase of velocity of impact load. In addition, the reduction of dimension of membrane can increase the dynamic response rather obviously.

Acknowledgments

This work was supported by the Natural Science Foundation of China (No.51178485) and Chongqing Municipal Construction Committee, Construction and Scientific 2014 Project No. 10-5.

References

Aksoylar, C., Omercikoglu, A., Mecitoglu, Z., Omurtag, M. H. (2012). Nonlinear transient analysis of FGM and FML plates under blast loads by experimental and mixed FE methods. Composite Structure 94: 731-744.

Balkan, D., Mecitoglu, Z. (2014). Nonlinear dynamic behavior of viscoelastic sandwich composite plates under non-uniform blast load: theory and experiment. International Journal of Impact Engineering 72: 85-104.

Belytschko, T., Lu, Y. Y. (1994). Element-free Galerkin methods. International Journal for Numerical Methods in Engineering 37: 229-256.

Chakravarty, U. K. (2012). Experimental and finite element modal analysis of a pliant elastic membrane for micro air vehicles applications. Journal of Applied Mechanics 79: 1-6.

Eshmatov, B. K. (2007). Nonlinear vibrations and dynamic stability of viscoelastic orthotropic rectangular plates. Journal of Sound and Vibration 300: 709-726.

Greschik, G., Mikulas, M. M. (2012). Design study of a square solar sail architecture. Journal of Spacecraft and Rockets 39: 653-661.

Guo, J. J., Zheng, Z. L. Wu, S. (2015). An impact vibration experimental research on the prestension rectangular membrane structure. Advances in Materials Science & Engineering 2015: 1-8.

Haddow, J. B., Wegner, J. L., Jiang, L. (1992). The dynamic response of a stretched circular hyperelastic membrane subjected to normal impact. Wave Motion 16: 137-150.

Hallquist, J. O., Feng. W. W. (1975). Dynamic response of axisymmetric hyperelastic membranes. Journal of Applied Mechanics 42: 890-891.

Jenkins, C. H., M. Korde, U. A. (2006). Membrane vibration experiments: An historical review and recent results. Journal of Sound and Vibration 295: 602-613.

Kapoor, H., Chun, S., Motley, M. R., Kapania, R. K., & Plaut, R., (2006). Nonlinear response of highly flexible structures to air blast loads: application shelters. Aiaa Journal 44: 2034-2042.

Kolsti, K. F., & Kunz, D. L., (2013). A point collocation method for geometrically nonlinear membranes. International Journal of Solids and Structures 50: 288-296.

Liu, C. J., Zheng, Z. L., & He, X. T., (2010). L-P perturbation solution of nonlinear vibration of prestressed orthotropic membrane in large amplitude. Mathematical Problems in Engineering 2010: 242-256.

Liu, C. J., Zheng, Z. L., & Yang, X. Y., (2013). Nonlinear damped vibration of pre-stressed orthotropic membrane Structure under Impact Loading. International Journal of Structural Stability and Dynamics 14: 133-146.

Nagaya, K., (1978). Vibrations and dynamic response of membranes with arbitrary shape. Journal of Applied Mechanics 45: 153-158.

Nayfeh, A. H., (1981). Introduction to perturbation techniques. John Wiley Sons, New York.

Yang, S., & Sultan, C., (2016). Modeling of tensegrity-membrane systems. International Journal of Solids and Structures 82: 125-143.

Young, L. G., Ramanathan, S., Hu, J., & Pai, P. F., (2005). Numerical and experimental dynamic characteristics of thin-film membranes. International Journal of Solids and Structures 42: 3002-3025.

Zheng, Z. L., Song, W. J., & Liu, C. J., (2012). Study on dynamic response of rectangular orthotropic membranes under impact loading. Journal of Adhesion Science and Technology 26: 1467-1479.